Optics Letters

Optimized laser-written ZBLAN fiber Bragg gratings with high reflectivity and low loss

Gayathri Bharathan,* Toney Teddy Fernandez, Martin Ams, Robert I. Woodward, Darren D. Hudson, and Alex Fuerbach

Faculty of Science and Engineering, MQ Photonics Research Centre, Macquarie University, NSW 2109, Australia
**Corresponding author: gayathri.bharathan@students.mq.edu.au*

Received 6 November 2018; revised 13 December 2018; accepted 14 December 2018; posted 17 December 2018 (Doc. ID 351186); published 14 January 2019

We report the direct femtosecond laser inscription of type-I fiber Bragg gratings (FBGs) into the core of soft-glass ZBLAN fibers. We investigate and compare various fabrication methods such as single pass (line by line), double pass, and stacking (plane by plane) to create the highest reflectivity FBGs (99.98%) for mid-infrared (mid-IR) applications. In addition, we experimentally demonstrate how the parameters that influence the coupling coefficient, i.e., refractive index modulation and overlap factor, can be controlled in these gratings to specifically tailor the FBG properties. The performance of the direct-written type-I gratings after 6 h of annealing is further analyzed, and the reflectivity increases by approximately 10 dB. To the best of our knowledge, this is the first demonstration of temperature-stable mid-IR FBGs with highest coupling coefficient (464 m^{-1}) and lowest loss (<0.5 dB/cm) without the use of an expensive phase mask.

https://doi.org/10.1364/OL.44.000423

Femtosecond (fs) laser inscription of integrated photonic components inside various transparent materials has evolved into an active research field over the last two decades [1]. In this method, different glass materials are translated relative to the tight focus of a fs laser beam. As a result of this irradiation, the material experiences a structural modification, leaving behind a localized permanent change in the refractive index [2]. The fs laser direct-write technique provides great flexibility, as various parameters such as pulse duration, pulse energy, repetition rate, wavelength, translation speed, focusing conditions, and target material composition can be adjusted individually, to optimize the inscription process [3,4]. A variety of devices such as waveguides, directional couplers, Bragg gratings, in-fiber polarizers, and waveguide lasers were successfully integrated into bulk glasses and fibers using this technique [5–10]. Among these devices, fabrication of fiber Bragg gratings (FBGs) is an active research field in the development of advanced fiber laser systems. Direct FBG inscription provides full flexibility in selecting the Bragg wavelength, order of the grating, and length of the grating in contrast to the expensive custom-made phase mask method [11].

Fiber lasers are a powerful tool to generate light at mid-IR wavelengths. Mid-IR fiber lasers in the 2.5–5 μm wavelength range have great potential to play a pivotal role in numerous applications such as spectroscopy and medicine, since the photon energies overlap with the strong vibrational molecular resonances of various atmospheric gases as well as water isotopologues [12,13]. The non-existence of fiber-coupled optical components at these wavelengths severely limits the ability to build highly efficient alignment-free, low-loss all-fiber laser cavities. Recent studies revealed that mid-IR laser systems with butt-coupled bulk mirrors suffer from optomechanical failure at high power levels [14,15]. However, replacing these bulk mirrors with FBGs enabled the realization of an alignment-free high-power mid-IR laser system with long-term robust operation [16]. FBGs are efficient wavelength selective components that can be integrated into mid-IR laser cavities to serve as mirrors, thereby forming true all-fiber laser systems [11,16,17,18]. However, the net reflectivity of the gratings and their out-of-band losses are key parameters in laser applications that directly affect the threshold and slope efficiency.

The FBG reflectivity can be tailored by varying the grating's coupling coefficient κ and/or physical length L [19]. For example, Fortin *et al.* demonstrated a 30 W fluoride glass all-fiber laser using a 99% reflective grating of 20 mm physical length [18]. Aydin *et al.* demonstrated a 41.6 W continuous-wave laser at 2824 nm based on a 30 mm long intra-core FBG with 99.5% reflectivity [20]. In both cases, the estimated κ was 150 m^{-1} and 111 m^{-1}, respectively. Bernier *et al.* inscribed a Bragg grating of 8 mm physical length in erbium-doped fluoride fiber to realize a highly stable all-fiber laser at 2824 nm, and the estimated κ was 272 m^{-1} [21]. This reveals that the coupling coefficient is a critical parameter that allows for a direct comparison of FBGs with different lengths. With a lower coupling coefficient, longer FBGs are required to achieve high reflectivity. However, while high coupling coefficients have been achieved using the phase mask FBG fabrication technique, the optimum κ values reported in ZBLAN fibers using direct-write inscription were <60 m^{-1} [11,15]. It is therefore an open question as to how to optimize the fs laser inscription process to yield high-reflectivity low-loss FBGs that can be written without requiring a phase mask.

This Letter provides a roadmap to the fs laser inscription of low-loss, high-reflectivity, and narrowband type-I FBGs in

ZBLAN fibers using direct fs laser inscription. Various fabrication techniques such as single pass, double pass, and stacking were analyzed to tailor different grating parameters such as refractive index modification and mode overlap factor to obtain a high coupling coefficient. This systematic study allowed us to fabricate FBGs in fluoride fibers with the highest coupling coefficient and ultra-low losses using direct fs laser inscription. In addition, thermal annealing was performed at 150°C, where the viscosity of the ZBLAN drops to 10^{13} P [22], for 8 h to ensure the stability of the type-I FBG's spectral response for high power mid-IR laser applications.

The quantitative characteristics of FBGs can be calculated from coupled-mode theory. In an FBG, the guided light undergoes minute Fresnel reflections from every interface of the periodic refractive index modulation. If all these reflections are in phase, they combine constructively, and the grating reflects a narrow wavelength range from the incident light wave with a center wavelength known as Bragg wavelength $\lambda_B = 2n_{\text{eff}}\Lambda/m$ [19], where m is the grating order, n_{eff} is the effective modal refractive index of the propagating mode, and Λ is the physical pitch of the refractive index perturbation. In the case of an FBG with a uniform period, the peak linear reflectivity of the grating (R) can be expressed in terms of κ and L [19]:

$$R = \tanh^2(\kappa L), \tag{1}$$

where κ is a measure of grating strength. The coupling coefficient between the FBG's two counter-propagating guided modes depends on the refractive index modulation (Δn), mode overlap factor (η), and Bragg wavelength [23,24]:

$$\kappa = \frac{\pi \Delta n \eta}{\lambda_B}. \tag{2}$$

The mode overlap factor is the fraction of the guided mode field power within the physical cross section of the FBG's refractive index perturbation. Techniques to control Δn and η are discussed in the following sections.

In this experiment, we inscribed FBGs into the core of a passive ZBLAN fiber with a core diameter of 9 μm, cladding diameter of 125 μm, and a numerical aperture (NA) of 0.2. A 1 kHz repetition rate Ti:Sapphire laser was used for FBG fabrication. This laser emits pulses centered at a wavelength of 800 nm with pulse duration of 130 fs in a linearly polarized Gaussian beam with $M^2 < 1.3$. The fiber was mounted onto a set of computer controlled *xyz* air-bearing stages (Aerotech ABL1000) and translated transversely through the focus of the laser beam in a rectangular pattern to obtain the grating structures [25]. To achieve optimum FBG inscription conditions, microscope objectives with different NAs and working distances were used in the experiment to precisely control the size and shape of the fabricated grating planes. The diameter of the laser beam at the entrance aperture of the objectives was 4.8 mm. During a parameter scan, short gratings were inscribed with varying pulse energies between 20 nJ and 150 nJ with various inscription speeds from 20 μm/s to 130 μm/s. Differential interference contrast (DIC) microscope images of the FBGs provide a fast initial assessment of the laser-inscribed lines and their potential to result in a low-loss grating.

In general, high NA objectives provide tight focusing conditions to modify the refractive index inside the sample. Therefore, the fs laser pulses were focused using a 50× oil-immersion objective with high NA (NA = 0.9, NA_{eff} = 0.65) and a 40× dry objective with NA and NA_{eff} of 0.6 and 0.56, respectively. Figures 1(a)–1(d) show a set of DIC images of the longitudinal cross section of the gratings fabricated inside the core of the passive ZBLAN fiber with the 40× dry objective at various writing speeds from 20 μm/s to 120 μm/s with 125 nJ of energy. As the speed increases, the pulse overlap decreases, and the modifications become more irregular, which introduces scattering losses in the gratings [see Figs. 1(c) and 1(d)]. Therefore, we used an inscription speed of 20 μm/s, which produced sufficient spatial overlap between consecutive pulses to achieve a smooth and continuous structure inside the fiber core, as shown in Fig. 1(a). In general, for all objectives used, we found that only a very narrow range of pulse energies and inscription speeds result in smooth gratings. Therefore, pulse energy and/or speed cannot be used to tailor the grating properties but must be chosen very carefully.

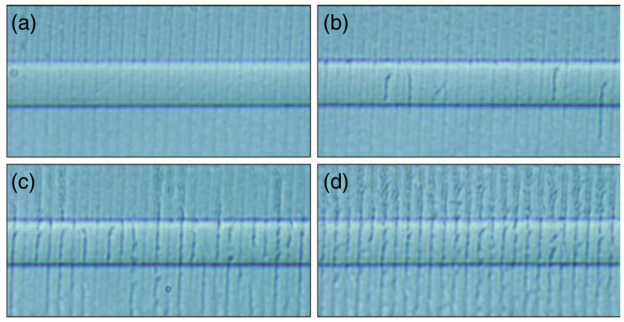

Fig. 1. Microscopic image of the FBG (top view) for various translation speeds: (a) 20 μm/s, (b) 40 μm/s, (c) 80 μm/s, and (d) 120 μm/s.

For an estimation of the coupling coefficient and overlap factor, FBGs were written with a physical length of 5 mm using a single-pass method (line by line), where the fs laser beam passes over the fiber once to fabricate the grating, as shown in Fig. 2(a). Various gratings with orders $m = 2$, 3, 4, and 5 were inscribed using both 0.9 NA 50× oil-immersion objective and 0.6 NA 40× dry objective, respectively. Later, a detailed spectral characterization of the FBGs was performed utilizing a broadband supercontinuum source with power stability better than ±1%. The collimated output of this source (Gaussian beam with $M^2 < 1.1$) was focused into the core of the fibers containing the FBGs using a ZnSe lens with a focal length of 6 mm. The transmission characteristics of the FBGs were then recorded using a mid-IR optical spectrum analyzer of 100 pm

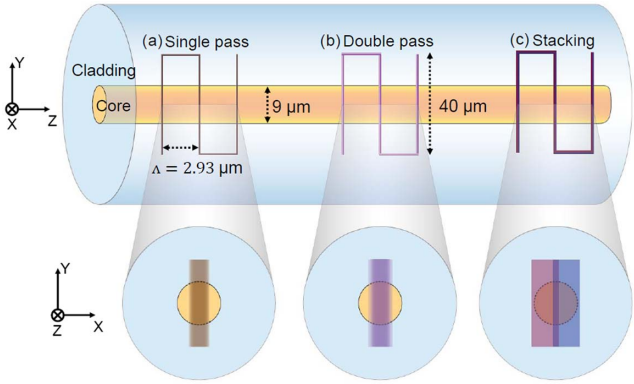

Fig. 2. Longitudinal and transverse cross sections of various inscription techniques: (a) single pass, (b) over pass, and (c) stacking.

resolution, ±0.5 nm wavelength accuracy, and ±0.2 dB power level accuracy. Due to the negligible losses in these type-I gratings, the reflectivity values could then directly be extracted from the measured transmission spectra. After spectral characterization, the FBGs were cleaved across the modified region of the fiber to observe the end facet under a microscope, which provided an estimate of the modal overlap factor (see Fig. 3 inset). Further, κ was calculated from the observed reflectivity and the length of the grating using Eq. (1).

The second-order grating inscribed with dry objective has a κ of 170 m^{-1}, which is lower than that of the grating produced by the oil-immersion objective (260 m^{-1}). This can be explained by an overlap of adjacent grating planes because of the increase in the irradiated volume. In the third-order gratings, the dry objective results in an approximately 40% duty cycle square wave refractive index profile, as well as a 60% modal overlap factor. Here, the duty cycle refers to the modification/space ratio of an individual grating period [24]. This enables a significant increase in the coupling coefficient in third-order gratings. In Fig. 3, it is evident that the third-order gratings result in the maximum coupling coefficient for both the objectives, and this observation is the maximum reported $\kappa = 380$ m^{-1} in fluoride fibers for the non-phase mask technique. The total time required to inscribe a 5 mm third-order grating was approximately 2.5 h. As can be seen in Fig. 3, the 0.6 NA 40× dry objective results in strong gratings, except for the second-order grating. Therefore, in order to obtain an optimum grating with desired overlap factor and coupling coefficient, we used the 40× dry objective in all further experiments. In the case of fourth- and fifth-order gratings, the number of grating planes for a given FBG length decreases with the increase in the order, resulting in a continuous reduction in the coupling coefficient and reflectivity.

For the development of high efficiency, alignment-free all-fiber laser systems, highly reflective thermally stable FBGs are required. Therefore, the investigation of the thermal stability of FBGs in ZBLAN fiber is crucial for high-power applications. In general, the core temperature of the ZBLAN fibers can exceed 100°C at high pump powers [20], which is lower than the glass transition temperature of ZBLAN glass, which is approximately 260°C [22]. For study of the temperature stability, we inscribed a single-pass uniform grating (125 nJ) with $L = 13$ mm and $m = 3$ using the 0.6 NA 40× dry objective. The resulting transmission spectrum of the FBG before thermal annealing is shown in Fig. 4. It reveals a strong and sharp Bragg resonance with a transmission dip of −21.4 dB corresponding to $R = 99.6\%$ at 2895.8 nm with a full width at half maximum (FWHM) of 0.62 nm and an out-of-band loss of <0.2 dB. The FBG was then thermally annealed in an oven at 150°C continuously for 10 min. We observed a significant increase in the resonant peak strength to −29 dB and a blue shift in the grating wavelength to 2894.6 nm. Next, the FBG was annealed at 150°C in steps of 2 h to a total time of 8 h and we observed that the Bragg resonance stabilizes to −32 dB ($R = 99.98\%$) after 6 h. The Bragg wavelength shifted to 2893.8 nm, and the FWHM bandwidth increased to 1.08 nm, as depicted in Fig. 4; the losses remained constant. In contrast to previous reports using the phase mask method [8,16,20], our thermal annealing study revealed an increase in reflectivity and a blue shift in Bragg wavelength repeatedly. This could be due to an increase in refractive index modulation (Δn) after annealing of the grating planes. However, further investigations are required to completely explain this observation.

In addition to the single pass FBG inscription, two other fabrication techniques, double pass and stacking, were studied to experimentally demonstrate how the grating parameters Δn and η can be manipulated to obtain a strong FBG with higher κ. In double-pass grating inscription (inscription time: 5 h), the fs laser beam sweeps the fiber core twice vertically along the y axis at the same focal position in the center of the core as depicted in Fig. 2(b). When compared with single-pass inscription, the double-pass technique induces only a slight increase in Δn [estimated from Eqs. (1) and (2)] but does not affect η. In the stacking technique (plane by plane), we also double pass the inscription beam (inscription time: 7 h). However, during each of the two passes, the fs laser beam is now focused to a different position within the fiber core, which is an optimized offset of +0.75 μm and −0.75 μm from the center of the core, respectively. This ensures an adequate overlap between the individual modifications, thus increasing η but keeping Δn constant. Figure 2(c) shows the schematic cross-sectional view of the core, where it can be seen that the modification completely covers the entire core of the fiber. This provides a 100% modal overlap, which significantly increases the coupling coefficient and thereby increases its reflectivity. This illustrates the flexibility of the fs laser inscription technique to tailor various grating parameters. All three inscription methods were performed using both the 0.9 NA 50× oil-immersion objective and the 0.6 NA 40× dry objective, and the results are summarized in Table 1. From the table, two main observations can be extracted. First, in a 5 mm long FBG, the higher modal overlap can be obtained from the stacking technique, and the increase

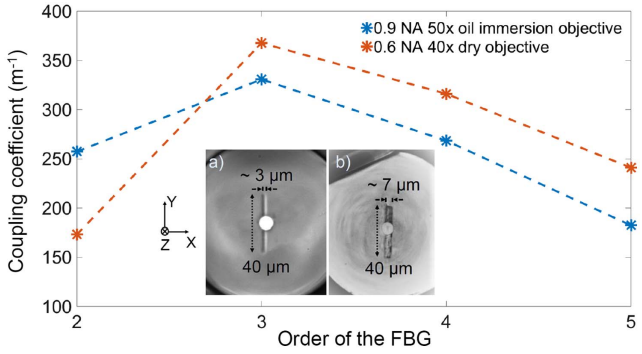

Fig. 3. Variation of κ with respect to grating order ($L = 5$ mm). The inset shows the cross section of the modification in fiber induced by (a) 0.9 NA 50× oil-immersion objective and (b) 0.6 NA 40× dry objective.

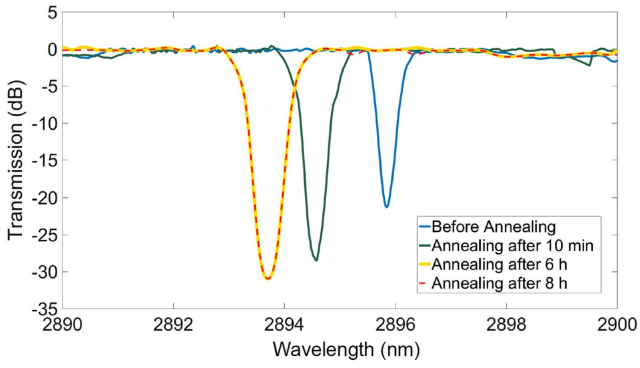

Fig. 4. Transmission spectra of a 13 mm long FBG before and after annealing at 150°C.

Table 1. Summary of the Various Grating Parameters (for Grating with Physical Length $L = 5$ mm) with Different Microscope Objectives and Inscription Techniques

Objective Used	Technique	Speed (μm/s)	Energy (nJ)	m	R (%)	$\Delta\lambda$ (nm)	Out-of-Band Loss (dB/cm)	κ (m^{-1})	Δ	η
0.9 NA 50× oil immersion	Single pass	20	65	3	86.4	0.72	0.10	330.7	1.2×10^{-3}	0.25
	Double pass	20	65	3	87.7	0.74	0.16	341.5	1.3×10^{-3}	0.27
	Stacking	20	65	3	94.4	0.98	0.26	423.6	1.0×10^{-3}	0.38
0.6 NA 40× dry	Single pass	20	125	3	90.1	0.78	0.18	367.6	5.7×10^{-4}	0.60
	Double pass	20	125	3	92.6	0.83	0.24	395.2	5.9×10^{-4}	0.62
	Stacking	20	125	3	96.2	1.04	0.34	463.8	4.3×10^{-4}	1

in κ (464 m^{-1}) or reflectivity (96%) is due to the increase in η. Second, the out-of-band losses increase with reflectivity for various inscription methods; however, the measured losses are always lower than 0.5 dB/cm.

Due to the high coupling coefficient of all gratings, it is difficult to fine-tune the reflectivity of the grating by simply changing the grating length. Therefore, the transversal extent of the inscribed lines was varied from 2.5 μm to 40 μm by varying the scanning distance in y direction (to control η) using the single scan technique, as depicted in the inset in Fig. 5, which shows that the coupling coefficient and reflectivity can be controlled effectively by varying the transversal size or mode overlap factor of the grating plane. Note that for the inscriptions $y = 2.5$ μm and $y = 5$ μm, the fs laser beam was programmed to be periodically blocked using a mechanical shutter, in order to prevent modifications in the core along the z axis, whereas in the other cases, the laser beam remained on throughout the fabrication process, as the z axis modification is present only in the cladding (see inset in Fig. 5).

In conclusion, we have demonstrated single-pass, double-pass, and stacking inscription techniques to optimize the reflectivity of direct-written FBGs in ZBLAN fibers. The results presented in this Letter show how the coupling coefficient, refractive index modulation, and mode overlap factor in type-I FBGs can be tailored using the fs laser direct-write technique. This is the first demonstration of high-reflectivity gratings with low loss (<0.5 dB/cm) and ultra-high coupling coefficients (464 m^{-1}) in ZBLAN fibers. Temperature stabilization of the grating was performed by annealing the grating at 150°C for 8 h, and we observed a significant increase in the strength of the Bragg resonance. This demonstration paves the way to the development of robust high-power, alignment-free, all-fiber mid-IR laser systems.

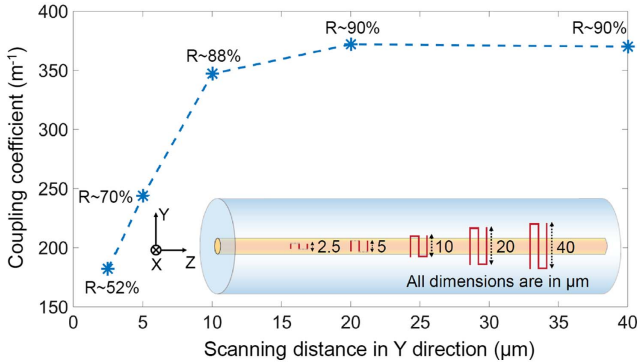

Fig. 5. Variation of κ with respect to the scanning distance in the y axis. Inset shows various widths in y axis along the length of the fiber. The experiment used FBGs with $L = 5$ mm.

Funding. Air Force Office of Scientific Research (AFOSR) (FA2386-16-1-4030); Australian National Fabrication Facility (ANFF) (OptoFab Node, NCRIS).

Acknowledgment. The authors would like to thank Professor Stuart Jackson for use of the OSA-Yokogawa.

REFERENCES

1. K. M. Davis, K. Miura, N. Sugimoto, and K. Hirao, Opt. Lett. **21**, 1729 (1996).
2. R. R. Gattass and E. Mazur, Nat. Photonics **2**, 219 (2008).
3. M. Ams, G. D. Marshall, P. Dekker, J. A. Piper, and M. J. Withford, Laser Photon. Rev. **3**, 535 (2009).
4. T. Fernandez, M. Sakakura, S. Eaton, B. Sotillo, J. Siegel, J. Solis, Y. Shimotsuma, and K. Miura, Prog. Mater. Sci. **94**, 68 (2018).
5. S. Gross and M. J. Withford, Nanophotonics **4**, 332 (2015).
6. H. L. Butcher, D. G. MacLachlan, D. Lee, R. R. Thomson, and D. Weidmann, OSA Contin. **1**, 221 (2018).
7. S. J. Mihailov, C. W. Smelser, P. Lu, R. B. Walker, D. Grobnic, H. Ding, G. Henderson, and J. Unruh, Opt. Lett. **28**, 995 (2003).
8. M. Bernier, D. Faucher, R. Vallée, A. Saliminia, G. Androz, Y. Sheng, and S. L. Chin, Opt. Lett. **32**, 454 (2007).
9. G. Bharathan, D. D. Hudson, R. I. Woodward, S. D. Jackson, and A. Fuerbach, OSA Contin. **1**, 56 (2018).
10. C. Wieschendorf, J. Firth, L. Silvestri, S. Gross, F. Ladouceur, M. J. Withford, D. J. Spence, and A. Fuerbach, Opt. Express **25**, 1692 (2017).
11. G. Bharathan, R. I. Woodward, M. Ams, D. D. Hudson, S. D. Jackson, and A. Fuerbach, Opt. Express **25**, 30013 (2017).
12. A. Schliesser, N. Picqué, and T. W. Hänsch, Nat. Photonics **6**, 440 (2012).
13. A. Vogel, J. Noack, G. Hüttman, and G. Paltauf, Appl. Phys. B **81**, 1015 (2005).
14. V. Fortin, F. Maes, M. Bernier, S. T. Bah, M. D'Auteuil, and R. Vallée, Opt. Lett. **41**, 559 (2016).
15. R. I. Woodward, M. R. Majewski, G. Bharathan, D. D. Hudson, A. Fuerbach, and S. D. Jackson, Opt. Lett. **43**, 1471 (2018).
16. F. Maes, V. Fortin, M. Bernier, and R. Vallée, Opt. Lett. **42**, 2054 (2017).
17. D. D. Hudson, R. J. Williams, M. J. Withford, and S. D. Jackson, Opt. Lett. **38**, 2388 (2013).
18. V. Fortin, M. Bernier, S. T. Bah, and R. Vallée, Opt. Lett. **40**, 2882 (2015).
19. T. Erdogan, J. Lightwave Technol. **15**, 1277 (1997).
20. Y. O. Aydin, V. Fortin, R. Vallée, and M. Bernier, Opt. Lett. **43**, 4542 (2018).
21. M. Bernier, D. Faucher, N. Caron, and R. Vallée, Opt. Express **17**, 16941 (2009).
22. I. R. Dunkley, R. W. Smith, and U. Varma, Ann. N.Y. Acad. Sci. **1027**, 150 (2004).
23. G. D. Marshall, R. J. Williams, N. Jovanovic, M. J. Steel, and M. J. Withford, Opt. Express **18**, 19844 (2010).
24. M. Ams, P. Dekker, S. Gross, and M. J. Withford, Nanophotonics **6**, 743 (2017).
25. S. Antipov, M. Ams, R. J. Williams, E. Magi, M. J. Withford, and A. Fuerbach, Opt. Express **24**, 30 (2016).